

Search for multiphoton events from proton-nuclei interactions at 300 GeV/c*

D. M. Stevens,[†] G. B. Collins, J. R. Ficenc, and W. P. Trower

Physics Department, Virginia Polytechnic Institute and State University,[‡] Blacksburg, Virginia 24061

J. Fischer and S. Iwata

Instrumentation Division, Brookhaven National Laboratory,[§] Upton, New York 11973

(Received 14 June 1976)

We have measured angular, energy, and multiplicity distributions of multiphoton events produced in proton-nuclei interactions at 300 GeV/c. The dominant features of these events are explained by known processes; however, a few multiphoton events inconsistent with known processes are found at a level at $\sim 10^{-7}$ per proton interaction.

I. INTRODUCTION

Since Dirac predicted the existence of magnetic monopoles¹ many fruitless experimental searches for free monopoles have been made.² Ruderman and Zwanziger³ explain these negative results by pointing out that the forces between monopoles are ultrastrong ($\alpha^{-1} = 137$) and long-ranged ($\sim r^{-2}$). Thus, monopoles which are produced from photons in pairs must have large velocities to escape each other's influence; however, bremsstrahlung processes associated with their creation may greatly exceed the monopole's rest energy. Thus, except for very-high-energy interactions, monopole pairs will remain virtual and their recombination would create additional radiation. The authors estimate that at incident photon energies of 10^{13} eV this process would produce showers containing ~ 100 photons with laboratory energies of a few hundred to a few thousand MeV.

In support of their model, Ruderman and Zwanziger point to the observation of anomalous energetic narrow pure photon cosmic-ray showers.⁴ A review of five events of this type shows that each contained 10–30 electron-positron pairs confined to a cone of 10^{-3} to 10^{-4} rad and with a total energy of >50 GeV.⁵ However, these multiphoton events could be due to other processes.⁶

Independently of interpretation, we have attempted to rediscover these anomalous multiphoton events. Although all the cosmic-ray events appear to have been produced by uncharged particles, circumstances at Fermilab made it necessary to use 300-GeV/c protons on a beryllium target as a source. The resulting photons were detected through the electromagnetic showers they produced in a lead converter placed before a set of three multiwire proportional chambers (MWPC).

The angular separation of individual photons was expected to be small, and accordingly the detector system was located at the largest possible distance

from the target, which for a separation of two wires in our MWPC's resulted in a resolution of about 10^{-4} rad.

The detector system was composed of a trigger and veto counters, lead and Plexiglas photon converters, and an air and a lead-glass Cherenkov counter. The trigger and subsequent tracking criteria, when combined with appropriately subtracted converter runs, enhanced the photon signal in the presence of an intense neutron background. Comparison with Monte Carlo-generated known photon processes allowed extraction of the anomalous multiphoton events.

II. EXPERIMENTAL DETAILS

A. Beam and targets

The experiment was performed in the *M-2* beam line of the Fermilab Meson Detector Building using a 300-GeV/c diffracted proton beam. This beam was produced at the completion of each main ring acceleration period by extracting a fraction of the circulating protons and focusing them on a target, $0.1 \times 0.1 \times 20$ cm³ Be. The resulting diffractively scattered protons then entered the *M-2* beam line, where they were transported 400 m and focused on our target. Here the beam area was 0.25×0.25 cm², had horizontal and vertical angular divergences of 0.1 mrad, and had an intensity variable from 10^5 to 10^7 protons per acceleration period. Our target, $1.3 \times 2 \times 20$ cm³ Be, was rotated with respect to the proton beam to obtain target thicknesses from 0.025 to 0.073 (0.033 to 0.098) interaction (radiation) lengths.

Figure 1 shows the three bending magnets downstream of the target that swept the unscattered proton beam and all produced charged particles clear of the detector. Between the last bending magnet and the detector, the charged beam was contained in a 7.6-cm-o.d. vacuum pipe located at 17.5 mrad with respect to the incident beam

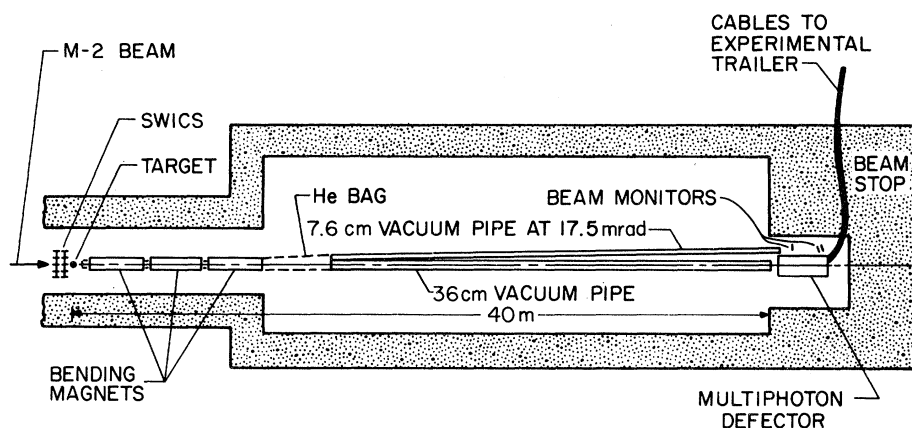


FIG. 1. Schematic of experimental setup.

direction. The unbent neutral secondaries were contained in a 36-cm-o.d. vacuum pipe.

An 8.9×8.9 -cm² scintillation counter placed at the downstream end of the 7.6-cm vacuum pipe monitored the beam at low intensities while a small counter telescope of two $5 \times 2.5 \times 1.3$ -cm³ scintillation counters located next to the detector monitored the high-intensity back-scattered particles from the beam dump.

The beam-spot position was monitored with survey-located horizontal and vertical single wire ionization chambers (SWIC's) read by a CAMAC system and displayed on a television monitor. The display was refreshed after each main ring cycle.

B. Multiphoton detector

The multiphoton detector of Fig. 2 converted individual photons into electron pairs, recorded

the electron tracks of the pairs, estimated the number of tracks, and measured the total energy of each multiphoton event. The detector consisted of three 248-wire MWPC's, an air and a lead-glass Cherenkov counter, and trigger and veto scintillation-counter arrays.

Each MWPC contained a vertical plane of 0.025-mm stainless steel readout wires spaced 1.6 mm apart. The details of the MWPC construction and operation appear as an appendix. The total average interaction length and radiation length for each chamber were 6×10^{-4} and 9×10^{-4} , respectively. The chambers had a 55-nsec time resolution using a gas mixture of 1% Freon 13B1, 82% ultrapure argon, and 18% methylal. Between data-taking runs the chambers were scanned using a motor-driven, highly collimated, remotely controlled source-scintillation counter and the resulting wire maps were evaluated for malfunctions. The efficiency of the chambers (99%) and the cluster size

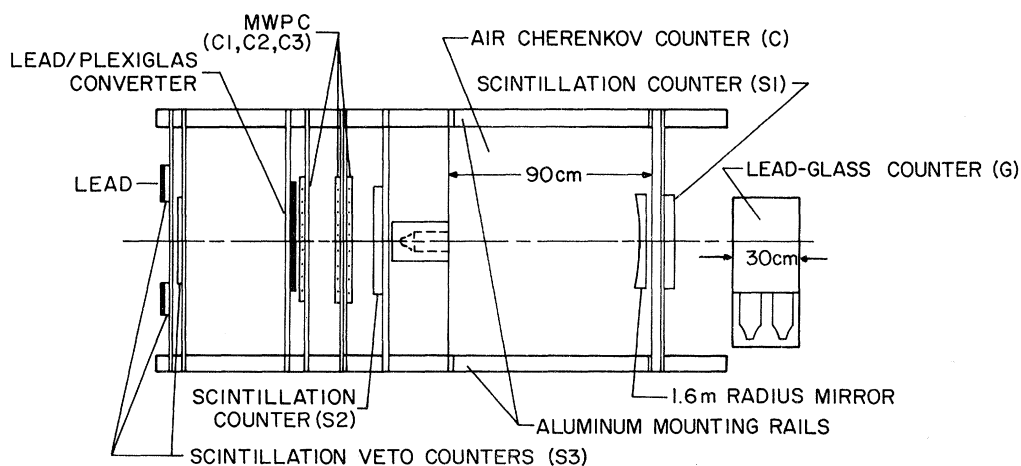


FIG. 2. Schematic of multiphoton detector.

(97% single wire) remained unchanged over the period of the experiment, 8 months elapsed time and 800 hours of operation.

The chamber signals were amplified, shaped, and output in a (1 V, 100 nsec) signal with a -1.75 -Vdc offset. Shielded coaxial cables 61 m long carried these signals to the interface located in the experimental trailer. A 70-nsec gate generated by the fast logic allowed latches to be set by the shaped in-time signals from the individual wires. The interface scanned all of these latches. If a set latch was encountered the memory buffer of the PDP-8/I stored the corresponding wire number. The interface scalars provided visual readouts of logic triggers, the number of times at least one latch was set, and the total number of latches set.

The air Cherenkov counter (C) detected only electrons produced by high-energy photons. The counter was a $90 \times 90 \times 90$ -cm³ box with sides of 0.5-cm Al and ends of 0.16-cm Al. A spherical mirror of radius 1.6 m collected Cherenkov light and focused it on a 12.7-cm phototube. Electrons with energy greater than 21 MeV and angle less than 35 mrad with respect to the mirror's symmetry axis (i.e. neutral beam line) produced detectable Cherenkov light. The counter detection efficiency for single particles was about 35%, or 58% for an electron-positron pair from a converted photon. Since the output pulse height of the phototube was correlated with the multiplicity of traversing charged particles it was fanned into five threshold discriminators, the lowest of which was set at the 1-2-particle level and used in the trigger logic while the others tagged higher-multiplicity events.

The lead-glass Cherenkov counter⁷ (G) consisted of a single piece of glass $45 \times 20 \times 30$ cm² viewed by two 12.7-cm phototubes located in a light-tight wooden box along the 30-cm dimension. The beam traversed the 30 cm while the vertical and horizontal acceptances were 20 cm and 45 cm, respectively. The counter was calibrated with 40-200-GeV/ c electrons and pions. Since the lead glass was 12 radiation lengths and 2 interaction lengths thick, electromagnetic showers developed completely while hadronic showers were only partially developed. Figure 3 shows this effect in the pulse-height spectrum from the summed phototube outputs, which was fanned into five threshold discriminators, the lowest of which was set for 100 GeV total shower energy and used in the trigger logic while the others tagged events of progressively higher energies.

The detector system, located 40 m downstream of the Be target, had a horizontal (vertical) acceptance of ± 4 (± 1.6) mrad defined by lead-covered scintillation counters preceding the detector which rejected events with charged particles or photons, outside the solid angle. Events with charged particles in the acceptance region were vetoed by a scintillation counter preceding the detector. Electromagnetic showers were produced by photons in a converter preceding the first MWPC. The system provided a high degree of selectivity toward high-multiplicity, high-energy, small-production-angle, low-cross-section, time-resolved individual events. At 40 m the MWPC wire separation provided a projected angular resolution of 0.04 mrad. We thus attempted to optimize the system's capability for detecting energetic, narrow photon showers.

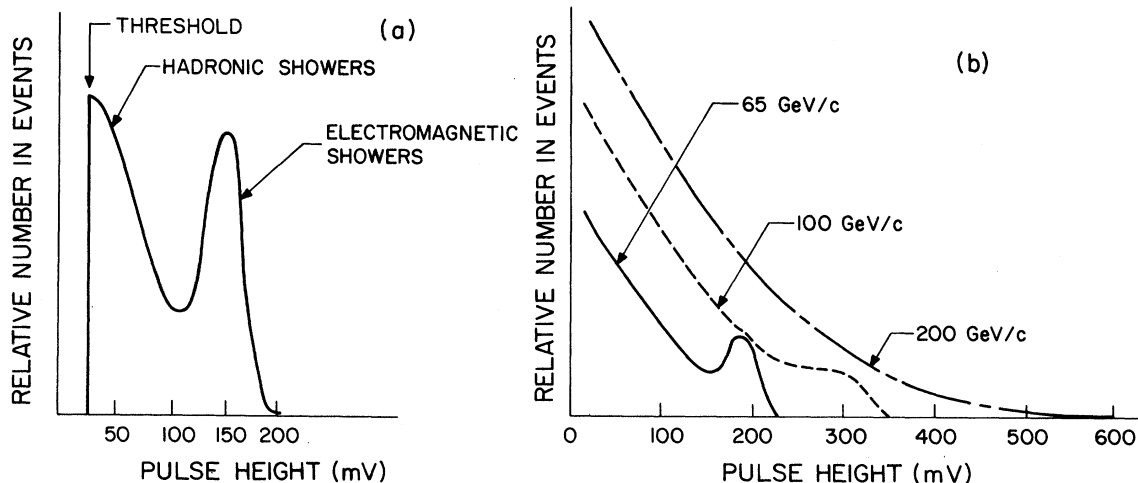


FIG. 3. Pulse-height distributions in the lead-glass counter for (a) 40-GeV/ c negative beam and (b) 65-, 100-, and 200-GeV/ c negative beams.

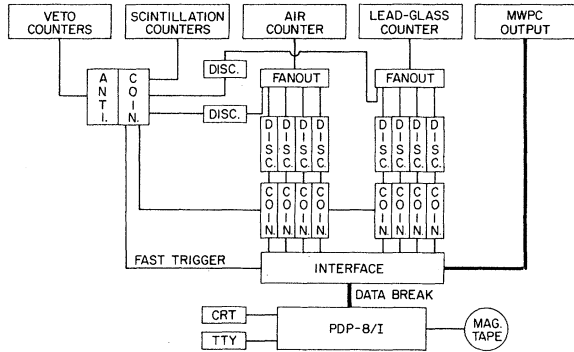


FIG. 4. Schematic of fast trigger logic, data acquisition, and on-line monitoring.

C. Event selection and acquisition

The fast logic, seen in Fig. 4, selected and recorded events with the required number of converted neutrals and minimum total energy. A trigger resulted when no veto counter signal (S3) was present but signals were obtained from both Cherenkov counters and their bracketing counters (S1 and S2). Thus our trigger ($S1 \cdot S2 \cdot C \cdot G \cdot \bar{S3}$), which required that an event contain ~ 3 forward, charged particles in the air counter and deposit at least 100 GeV in the lead-glass counter, generated a gate signal for the interface. If the signals were in the gate and if there was at least one hit on the third chamber, all chambers were scanned by the interface and the numbers of the hit wires were read through a data break into a PDP-8/I memory buffer.

The interface accepted eight additional bits of data from the air and the lead-glass counter discriminators. Since high discriminator levels indicated a large-number of electrons and high total photon energy, respectively, we could trigger on a low air and glass level to optimize the data acquisition rate while tagging events with high multiplicity and/or high energy.

The wire identification codes for hits on proportional-chamber wires were read serially into separate 12-bit words of the memory buffer, as were the Cherenkov-level codes. A typical event would have codes which corresponded to hits on the first, second, and third chambers, an air Cherenkov level, a lead-glass Cherenkov level, and an event-separation word of zeros. When the 1024-word data buffer was filled, the computer then copied the data buffer onto a 7-track 556 BPI magnetic tape and incremented the on-line analysis arrays.

D. Monitoring

On-line data were logged through the computer's data break. Thus, while data were being taken diagnostic displays were viewed on a storage scope; they included wire maps (frequency of hits on each MWPC), chamber multiplicity distributions (frequency of single, double, triple, etc. hits), and individual events. Wire maps and multiplicity distributions were updated after every full data buffer. A teletype provided, upon request, a hard copy of the distributions. These displays allowed a check on the detector performance and an overview of the data being acquired.

After each data tape had been filled, ~ 12 hours, it was transported to the CDC-6600 for analysis. Using the large sample of data, wire maps and multiplicity distributions as a function of the Cherenkov counters' levels could be obtained with good statistics. In addition, typically 100 events were displayed on hard copy, providing a highly visible sample of data and allowing us to examine in detail preselected categories of events. We thus were able to optimize the experimental arrangement for our search.

III. DATA ANALYSIS

The central experimental problem is to identify events with 10–30 photons with production angles from 0.1 to 1.0 mrad in the presence of multiphoton events from known multimeson-production processes, spurious events from misinterpreted neutron interactions, and apparatus malfunctions. Some 340 000 events were recorded; they were produced in a variety of ways, some expected and some spurious, but most may be considered as a background to the searched-for anomalous multiphoton events. The important sources of the background are now discussed.

Neutron-produced events were 60 times more copious in our detector than photon events.⁸ However, their ratio was reduced an order of magnitude because the lead-glass counter is inefficient in producing hadron-induced Cherenkov radiation. Furthermore, the probability of one or more photon conversions in the lead exceeds the neutron interaction probability by a factor of 30. Therefore the ratio of neutron triggers to total triggers is $< \frac{1}{5}$; for details see Table I. By using lead and Plexiglas converters whose interaction probabilities were nearly the same, we eliminated by a Plexiglas subtraction most of the effects of the remaining neutron events. However, 300-GeV neutrons which interact in the converter produce multiple neutral pions, $\langle n_{\pi^0} \rangle \sim 4$, whose photons will be converted more efficiently in lead than in Plexiglas. This effect is strongly topology-depen-

TABLE I. Estimated fraction of triggers.

Source	Converter	
	Lead	Plexiglas
n scintillator (S3)	0.018	0.062
n converter	0.165	0.550
γ converter	0.817	0.388

dent; it is smallest at large charged multiplicities.

Other backgrounds were multiplicity-dependent. The multiplicity, n , was determined by the number and location of MWPC hits. Figure 5 shows three events to illustrate the selection criteria. An acceptable track had to have hits on three chambers whose projected angle relative to the neutral beam axis was <10 mrad (i.e., one-wire separation on adjacent chambers). Adjacent tracks were required to be separated in C1 by at least two unhit wires.

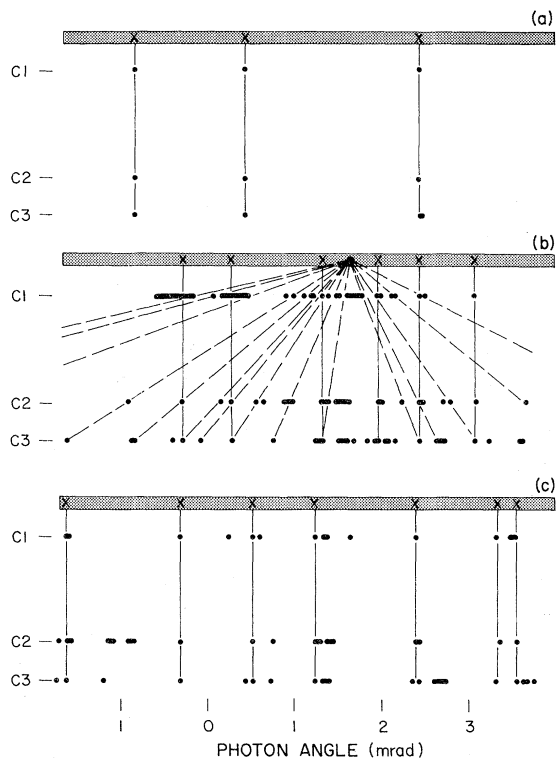


FIG. 5. Three typical events (number of showers, production angle, cone angle, total energy). Dots are MWPC hits, solid lines indicate the shower axes, and broken lines suggest trajectories of particles emitted at large angles from a single source for (a) a three-photon shower ($n=3$, $\theta_p=0.8$ mrad, $\theta_c=3.2$ mrad, $150 \leq E \leq 200$ GeV), (b) and erroneously identified event ($n=6$, $\theta_p=1.0$ mrad, $\theta_c=3.3$ mrad, $250 \leq E \leq 300$ GeV), and (c) a visually verified complex event ($n=7$, $\theta_p=0.9$ mrad, $\theta_c=5.2$ mrad, $150 \leq E \leq 200$ GeV).

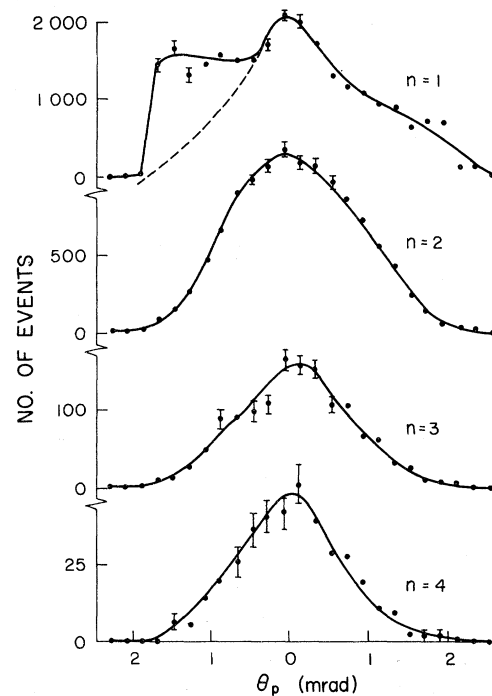


FIG. 6. Production-angle (θ_p) distributions for various photon multiplicities. The distortion in the $n=1$ distribution is attributed to single particles scattered from the deflected proton beam. The broken line represents the folded spectrum.

Photons interacting in the lead (Plexiglas) converter usually created a small shower since the converter was only 0.57 (0.037) radiation lengths. For a photon energy of ~ 1 GeV the angular separation of e^+e^- pairs is ~ 1 mrad and the shower was recorded as a single hit. Low-energy electrons are occasionally emitted from the shower at large angles but usually did not complicate the event interpretation. Figure 5(a) shows a three-track event. The requirement that the track be within ± 10 mrad of the neutral beam axis eliminated most photons not coming directly from the target.

Particle scattering from the apparatus was investigated by examining the shower production-angle (θ_p , defined as the average angle of the extremum tracks) distributions for various multiplicities. These are seen in Fig. 6 to be approximately Gaussian-distributed about 0 mrad except for $n=1$, whose asymmetry is attributed to the scattering of the proton beam which is to the left of 0 mrad. The effect of our veto counters is apparent in these distributions. For $n \geq 2$ the effects of scattering are not apparent in the distributions.

The veto counter, placed 56 cm in front of the first MWPC to eliminate stray charged particles, could have neutron interactions in its downstream

side producing unvetted charged secondaries and π^0 photons with $\theta_p < 10$ mrad. The Plexiglas subtraction did not completely eliminate the events with low charge multiplicity because of the difference in the photon conversion probabilities of lead and Plexiglas. Corrections for this effect were made using runs where the veto counter was not in the acceptance aperture. The distributions of cone angles (θ_c , the angle between extremum tracks) for various multiplicities are displayed in Fig. 7, where the effects of the veto counter are apparent in the $n=2$ distribution.

After tracking, subtraction, and correction, the remaining events were compared with events expected from known hadron processes. We used a " ρ -meson model" to obtain the number of neutral-pion pairs, and we proportionally added single neutral pions to obtain agreement with the bubble-chamber results⁹ for the average neutral-pion multiplicity for each topology. The momentum distribution was parameterized by the scaling function of Dao *et al.*¹⁰ Neutral pions produced diffractively through the decays were included:

$$N^*(1238) \rightarrow N\pi^0,$$

$$N^*(1760) \rightarrow N^*(1238)\pi^0 \rightarrow N\pi^0\pi^0,$$

and

$$N^*(1760) \rightarrow N\rho \rightarrow N\pi^0\pi^0.$$

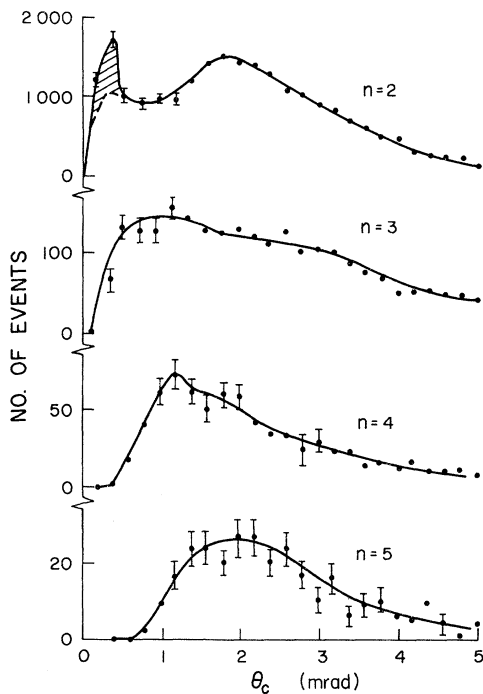


FIG. 7. Cone-angle (θ_c) distributions for various photon multiplicities. The shaded peak in the $n=2$ curve is attributed to neutrons interacting in the veto scintillator, S3.

For K_S^0 and K_L^0 decays into π^0 the bubble-chamber K_S^0 momentum distributions¹¹ were used.

The Monte Carlo events from known production processes constrained by the physical characteristics of the apparatus allowed us to evaluate the overall performance of the apparatus over a wide range of responses. Thus the estimated absolute counting rates for shower multiplicities of 1 through 4 were compared with the corresponding observed multiplicities. For $n \leq 3$ the good agreement between the Monte Carlo distribution and the data indicated that the experimental conditions were understood, so that high-multiplicity events where

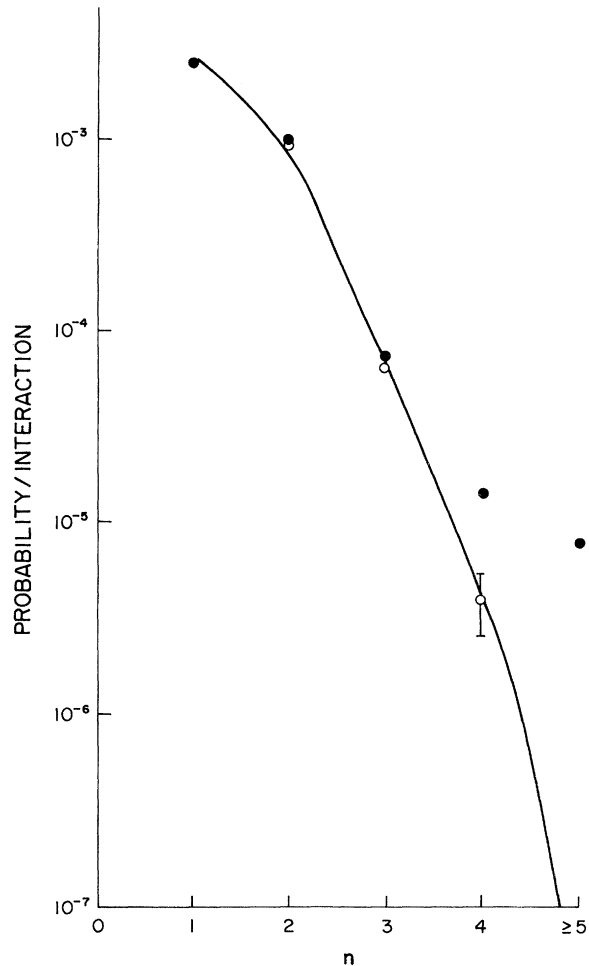


FIG. 8. Comparison between the fraction of observed photon multiplicities per interaction and the same for the generated data. All events have a total energy > 100 GeV. Solid line: generated data. ●: absolute cross sections resulting from lead-Plexiglas subtraction. ○: cross sections resulting from lead-Plexiglas subtractions, with the hit requirement, adjusted by a scale factor representing the fraction of events eliminated by that requirement.

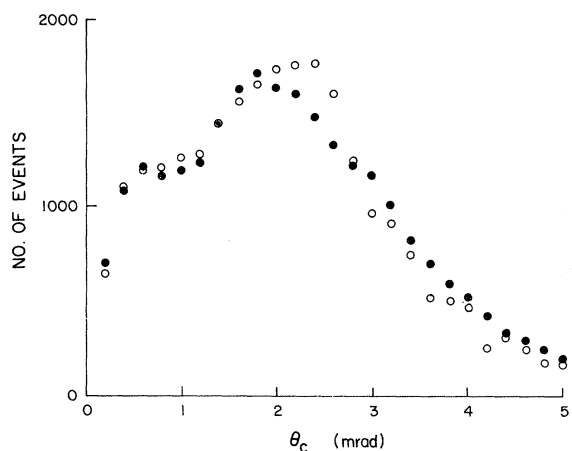


FIG. 9. Comparison between the cone-angle distributions of the data (●) and generated events (○).

the Monte Carlo distribution provides little information could be approached with some confidence.

The generated angular, energy, and multiplicity distributions were compared with distributions resulting from the subtracted data corrected

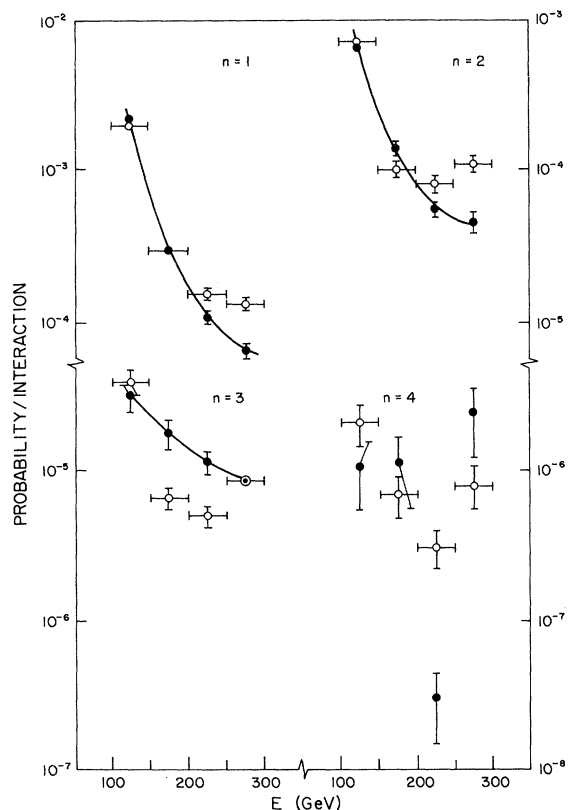


FIG. 10. Comparison between the energy distribution of data (○) and generated events (●) for various values of multiplicities (n) and the corresponding distributions for generated events adjusted as in Fig. 8.

for counter inefficiency (+4% to +45%), trigger and data-collection efficiency (+4%), and veto-counter effects (+15%). These comparisons *without* arbitrary normalization are shown in Figs. 8–10.

The multiplicity distributions in Fig. 8 are strikingly similar for $n < 4$, but there is some difference between the data and generated events for $n \geq 4$. The reconstruction program encountered difficulty with complex events. Neutron interactions in the converter can produce charged multiplicities as large as 20. When a large number of secondaries traversed the MWPC at large angles the hits could be so numerous that their accidental arrangement satisfied the selection criteria and a falsely high multiplicity resulted. The event in Fig. 5(b) was probably due to a single neutron interaction but was assigned for $n=6$. These events occurred relatively more frequently for the lead than for the Plexiglas converter because of different conversion and interaction properties. Thus, the subtraction procedure did not eliminate all these events.

To further reduce these effects a “hit requirement” was applied which demanded that the number of hits on the first chamber be less than four times the number of tracks identified. The multiplicity distributions for both the lead and Plexiglas converters with and without this hit requirement are shown in Fig. 11; the result is that all evidence for events with $n \geq 5$ is eliminated. All differences

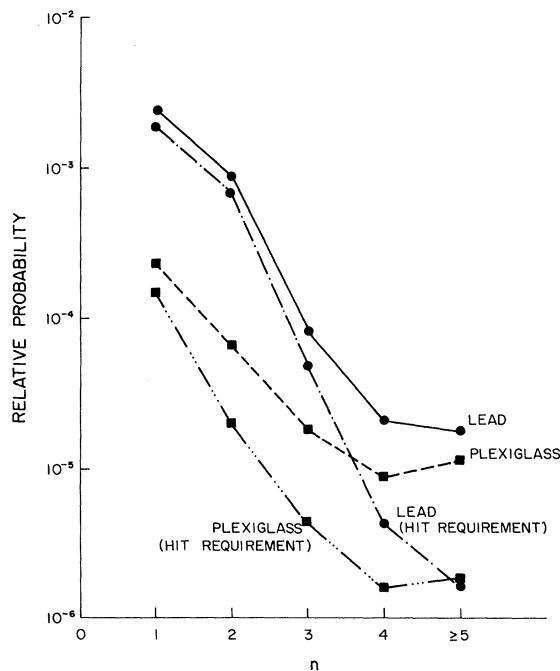


FIG. 11. Multiplicity distributions with lead and Plexiglas converters with and without the hit requirement. All events have a total energy > 100 GeV.

in Fig. 8 between the data and the generated events are removed by this requirement.

The θ_c distributions obtained from the generated and measured events are consistent, as seen in Fig. 9. The energy distributions, seen in Fig. 10, are inconsistent at high energy and low multiplicity. Since there are no measured π^0 or K^0 spectra at these high energies and small angles the generating functions may be in error.

Since the generated distributions predicted essentially no events with $n \geq 5$ and since we may have eliminated all events of the type we were searching for by the "hit requirement," we visually examined all such events. The criterion for accepting an event as genuine was the presence of five or more separate showers whose axes were parallel to one another so they could be associated with the beryllium target 40 m upstream. This selection eliminated nearer sources, which gave intense high-multiplicity divergent showers that were occasionally misinterpreted. The 588 such events from the lead converter gave 7 genuine events, while the Plexiglas has 334 events which yielded 2 genuine events.

If $\theta_c < 0.5$ mrad the photon-produced showers would overlap to some extent and the tracking criteria would record a multiplicity lower than the true one. For example, if a typical multiphoton event contained 20 photons within $\theta_c = 0.5$ mrad, we would record $n = 5$ less than 1% of the time although 90% of the events would have five or more photon conversions. To investigate these effects we individually examined all events which had numerous hits within a small region of the first chamber. These events were then assigned a multiplicity on the basis of their hit distributions in all three chambers. Of the 2646 events from the lead converter 4 were assigned $n \geq 5$, while none of the 991 events from the Plexiglas qualified.

Events from the lead converter selected by the two scans are given in Table II, while Fig. 5(c) shows one of them. Only one event has an energy < 150 GeV, while the average θ_c is greater than the 1 mrad seen in the anomalous cosmic-ray multiphoton events. After normalization and correction for trigger inefficiencies the 9 (11-2) events correspond to a cross section for production by protons on a nucleon of (6.5 ± 2.4) nb. This number has not been corrected for effects of the veto counter, aperture, tracking criteria, or conversion efficiency since the size of these corrections depends critically on the number of photons in a multiphoton event and their angular spread. Since these events have θ_c as large as 6 mrad these corrections can increase the estimated cross section by a factor of 4 or more. Therefore the cross section per nucleon for this residue is

TABLE II. Characteristics of individually scanned Pb converter events.

n	E (GeV)	θ_p (mrad)	θ_c (mrad)
7	150-200	0.92	5.16
6	150-200	1.04	2.12
6	100-150	0.52	5.76
7	150-200	0.72	4.00
6	200-250	1.12	3.72
5	250-300	0.64	1.64
6	250-300	1.24	4.92
5	150-200	2.36	3.08
6	200-250	2.40	1.04
6	150-200	3.36	0.72
6	200-250	0.10	0.52

estimated to be 0.5-30 nb if they are produced by proton interactions.

The multiphoton events seen in cosmic rays were apparently produced by either secondary neutrons or photons. If the residue is produced by neutron-Be interactions, assuming that the neutrons originate from proton collisions and are produced on the average at the center of the target, we find a cross section per nucleon of 2-200 nb. If the residue is produced by γ -Be collisions where the photons are produced in p -Be collisions in the same target, we estimate a cross section per nucleon of 0.02-1.2 mb. This latter number is to be compared with the estimated cross section per nucleon for multiphoton cosmic-ray showers⁵ of 3 mb, assuming $A \sim 100$ for emulsions. If the anomalous cosmic-ray multiphoton events were produced by cosmic-ray neutrons a production cross section per nucleon of 30 mb would be required, which is 1000 times greater than ours.

IV. CONCLUSION

The significance of these few high-multiplicity events must remain in doubt since they represent processes occurring only about twice in 10^7 p -Be interactions. Further experimental investigation is required to establish the existence of these events and possibly their nature and course.

ACKNOWLEDGMENTS

We thank J. Gatz, F. Meredith, S. Rankowitz, and the personnel of the machine shop of the Instrumentation Division at BNL for their support in this experiment. We gratefully acknowledge P. Koehler and H. Haggarty of Fermilab for the exceptional services they provided which materially contributed to the successful completion of this experiment. The machine shop, supervised by L. Barnett, and the electronics shop, supervised

by A. Wyrick, at VPI & SU designed and constructed many of the components of the experiment.

APPENDIX: MULTIWIRE PROPORTIONAL CHAMBERS FOR HIGH-ENERGY MULTIPHOTON DETECTION

1. Requirements

The role of MWPC's in this experiment was to measure the coordinates of showers, which were frequently one or more unresolved electron pairs. The number and spatial coordinates (in one dimension) of the converted photons are thus obtained. MWPC's were used because of their high multiparticle efficiency, good spatial resolution, and good time resolution which prevented a high background of random counts from being interpreted as a multiparticle event. The MWPC transparency left the charged and uncharged particles largely unaffected so that other downstream detectors, such as Cherenkov counters, could give meaningful results. The chambers were designed to obtain high efficiencies with a minimum of spurious events, making large redundancy unnecessary.

The characteristics of the multiphoton events searched for set the following requirements on the MWPC's:

(a) *High efficiency for detecting an unresolved electron pair.* Since the opening angle for an electron pair produced by a 50-GeV photon is ~ 0.02 mrad it will be an unresolved pair which preserves the direction of the original photon. Even an efficiency of 90% for detecting a single minimum-ionizing particle results in an efficiency of 99% for detecting one of the pair.

(b) *Low efficiency for detecting bremsstrahlung x and δ rays.* A high-energy photon is identified by a straight track almost parallel to the beam direction, while soft components produce tracks which do not have a high directionality, which makes it difficult to identify individual pairs in a multiphoton event.

(c) *High spatial resolution.* Angular separations as small as 10^{-4} rad (corresponding to a 4-mm separation at the detector) could result from the multiphoton events of interest. Thus the highest

possible resolution is needed to distinguish the individual photons.

(d) *Good time resolution.* Temporal resolution is necessary to avoid extra tracks due to accidental coincidence generated by the large neutron background.

2. Chamber construction

Four chambers satisfying the above requirements were constructed with the characteristics listed in Table III. Since spatial resolution is proportional to wire spacing the latter was made as small as possible, 1.6 mm, consistent with good efficiency. Each chamber was constructed from four fiberglass G-10 frames of 61×61 cm². One end of the anode wires was soldered to a printed circuit board which fanned into 31 groups of 8 wires, each group having a multipin connector. The cathode wires were treated in a similar way; however, they were fanned into three groups, each of which was connected to a high-voltage cable through a 120-M Ω resistor. No guard wires or strips were used. Window edges adjacent to the high-voltage plane were concave in shape to inhibit breakdown.

A 3-mm O-ring groove cut into the faces of three frames provided a gas-tight fit. With O rings in place, the plane faces were coated with RTV (General Electric silicone glue) and bolted together before the RTV sealer cured. The chamber was then bolted to an aluminum backing plate, which had a 42×42 -cm² window, to provide rigidity and facilitate chamber mounting. There were two input (output) gas ports at the bottom (top) of the active area.

3. Readout electronics

The electronics consisted of three types: transmitter cards located on the chamber, receiver cards located at the input of an interface, and the computer interface. The anode wires of the MWPC's were operated at a -1.2 -V dc bias to reduce noise.

Chamber signals were amplified, discriminated, and shaped in the transmitter card, which was made of discrete components and was plugged into the connectors on the chamber. The characteristics of the transmitter cards are listed in Table IV.

The standardized output pulse was carried through a 61-m coaxial cable to the interface. The cables, grouped by 16 wires, were lashed together and covered with a shield. The cable delay allowed the fact logic to decide if data were to be scanned.

Each of the signal cables was fed into a single receiver card which functioned as a fast gate and

TABLE III. Chamber construction characteristics.

Chamber gap	2 \times 9.5 mm
Anode wire	25- μ m stainless steel
Anode-wire spacing	1.6 mm
Cathode wire	100- μ m stainless steel
Cathode-wire spacing	1.27 mm
Windows	125- μ m Mylar sheets
Window-cathode spacing	6.4 mm
Active area	40 \times 40 cm ²

TABLE IV. Performance of amplifier discriminator cards.

Threshold for negative wire pulse	1.5 ± 0.7 mV
Threshold for positive pulse	>40 dBm
Proportional delay (for ×3 overdrive)	27 ± 3 nsec
Time slewing	
from ×1 to ×3 overdrive	10 nsec
from ×3 to ×10 overdrive	2 nsec
Output pulse width	
near threshold	80–90 nsec
from ×2 to ×8 overdrive	45–60 nsec
Overall timing uniformity at ×3 overdrive	±6 nsec

a latch. The minimum gate width was adjustable by an external cable connection. The interface scanned all of the MWPC latches. If a latch had been set it stored the corresponding wire number in the memory buffer of a PDP-8/I computer.

The interface provided several selective options: multiplicity of wires hit, number of wires scanned, number of words transferred to the computer before program interruption, external/internal gate mode, and data bits from other detectors. The interface was also equipped with triggers which provided visual readouts of logic triggers, the number of times at least one latch was set, and the total number of latches set.

4. The gas mixture

The gas mixture was of critical importance in achieving the desired chamber characteristics. Considerable care was taken to obtain, simultaneously, good efficiency and rapid falloff of efficiency with delay time to obtain good time resolution.

The MWPC's were tested using traversing β

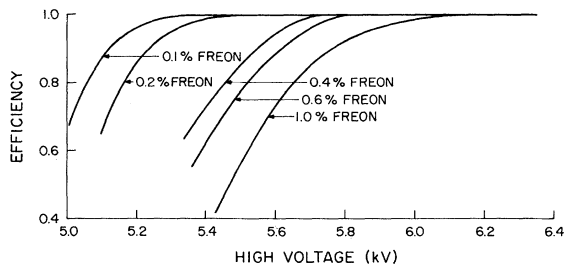


FIG. 12. Measured efficiency versus voltage with various amounts of Freon for a minimum ionizing particle. A 0.5-mV discriminator threshold and a 70-nsec gate pulse width were used.

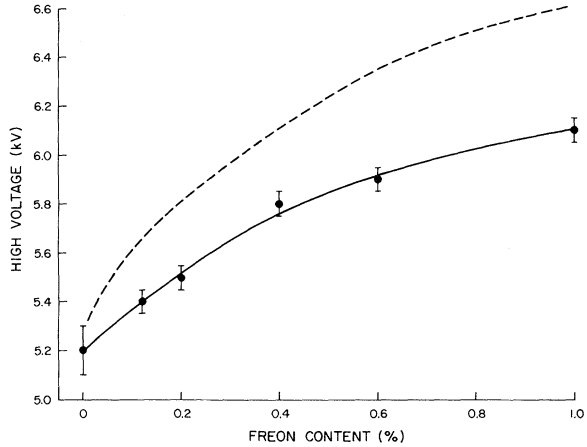


FIG. 13. Beginning of efficiency plateau (solid line) and Geiger discharge (dashed line) as a function of the Freon content.

rays selected by a scintillator. The chamber was flushed with the gas mixture, 82% Ar and 18% methylal, to which various amounts of Freon 13B1 were added. Without the Freon the efficiency plateau nearly overlapped with a breakdown region, making the whole gas volume sensitive. The Freon eliminated the breakdown problem and provided operating voltage limited only by Geiger discharge. The efficiency curves for various amounts of Freon between 0.1% and 1% are shown in Fig. 12 as a function of the high voltage. Figure 13 shows the beginning of the efficiency plateau and the Geiger discharge. The error bars reflect nonuniform performance of the transmitter cards and anode wire gain. For Freon contents of up to 1%, (99±1)% efficiency for minimum-ionizing particles was obtained, which compares favorably with magic-gas results, where the maximum

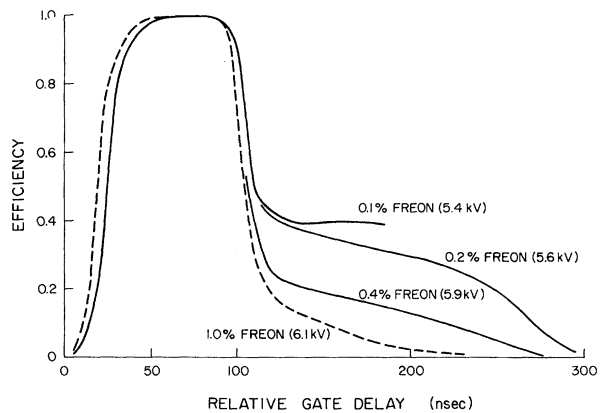


FIG. 14. Timing curves of chamber signals measured with 70-nsec gate showing the occupation time of the anode wire.

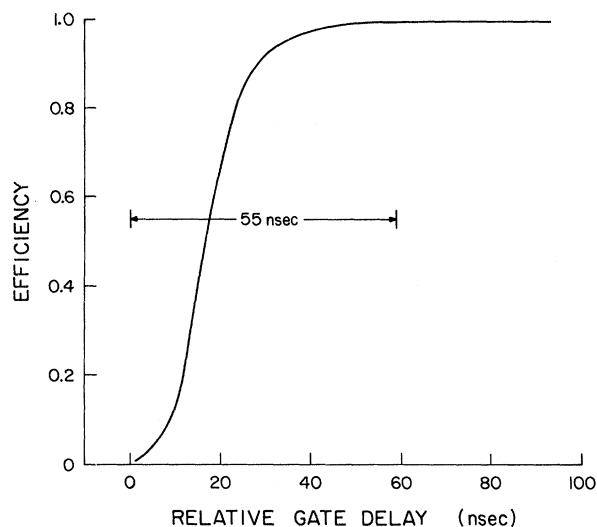


FIG. 15. Integral timing curve of chamber signals with 1% Freon showing the minimum gate width to obtain 100% efficiency.

amount of Freon to achieve nearly 100% efficiency for our particular wire spacing (1.6 mm) would be about 1.3%.¹² Thus, increasing the percentage of Freon provides full efficiency while increasing the plateau width of the operating voltage.

Figure 14 shows timing curves measured with a 70-nsec-wide gate. After the full efficiency peak an appreciable tail exists, which decreases the chamber's resolving time and thus gives rise to accidental coincidences. The tail does not show up in a time-jitter spectrum measured with fast OR signals. However, the usual measurement of the time-jitter spectrum does not show a true occupation time of the anode wire and overestimates

the chamber performance. The height of the tail decreased with the increasing Freon content faster than it increased with voltage. Increasing the discriminator threshold by a factor of 3 reduced the tail to about half that shown in the Fig. 14, with only a 1–2% decrease in efficiency peak. In fact, at the output of the transmitter card the late pulses were wider, indicating smaller input amplitudes. Thus, in addition to the nearest ionization clusters contributing to the efficiency peak, those produced far from the wire still contribute, especially when the Freon concentration is <0.4%. Heavy positive ions produced in the first avalanche reduce the multiplication factor for the electrons which survive capture.

We chose 1% Freon because it produces the smallest tail in the timing curve and the largest efficiency plateau. The resulting multiplicity was 97% on one wire and 2% on the two adjacent wires. A larger amount of Freon may have provided good efficiency, but the operating voltage would have had to be unpleasantly high. The minimum gate width for 100% efficiency with 1% Freon was measured to be 55 nsec by delaying a 180-nsec-wide gate pulse, thus increasing a time overlap with the chamber pulse, and is seen in Fig. 15.

In conclusion, the characteristics of a multi-wire proportional chamber required for multiphoton detection were realized by a gas mixture which contained a fairly large amount of electronegative gas: 1% Freon 13B1, 82% Ar, and 18% methylal. Most of the requirements could be satisfied with less Freon; however, the substantial efficiency long after particle passage, which was observed in the differential timing curve and is not revealed by the conventional time-resolution measurement, was substantially reduced.

*This work was performed at the Fermi National Accelerator Laboratory, which is operated by Universities Research Associates, Inc., under contract with the U. S. Energy Research and Development Administration.

†Work presented in partial fulfillment of the requirements for the Doctor of Philosophy degree at Virginia Polytechnic Institute and State University. Present address: Babcock and Wilcox, Lynchburg, Virginia.

‡Work supported in part by grants from the Research Corporation of New York and the National Science Foundation.

§Work supported by the U. S. Atomic Energy Commission.

¹P. A. M. Dirac, Proc. R. Soc. London **A133**, 60 (1931).

²The literature on magnetic monopoles is summarized by D. M. Stevens in VPI Report No. VPI-EPP-73-5 (unpublished).

³M. Ruderman and D. Zwanziger, Phys. Rev. Lett. **22**,

146 (1969).

⁴M. Schien, D. M. Haskin, and R. G. Glasser, Phys. Rev. **95**, 855 (1954); **99**, 643 (1955).

⁵G. B. Collins, J. R. Ficenec, D. M. Stevens, and W. P. Trower, Phys. Rev. D **8**, 982 (1973).

⁶For example, cascade decay by photon emission of closely spaced nucleon resonances: V. L. Teplitz and K. Johnson, private communication; F. von Hippel and C. Quigg, Phys. Rev. D **5**, 624 (1972).

⁷Graciously lent on short notice by John W. DeWire of Cornell University.

⁸In all discussions in this paper hadronic cross sections are taken to be $39A^{2/3}$ mb, where A is the mass number of the target. We assume that the forward charged- and neutral-secondary spectra are the same for p - A as for pp and that np and nn interaction are the same as pp except for one and two fewer charges, respectively. We also assume, as an upper limit, that 40% of all p -Be interactions produce a neutron in our de-

tector. The photon numbers used here will be discussed later in the text.

- ⁹F. T. Dao, D. Gordon, J. Lach, E. Malamud, J. Schivell, T. Meyer, R. Poster, P. E. Schlein, and W. E. Slater, *Phys. Lett.* 45B, 73 (1973).
- ¹⁰F. T. Dao, D. Gordon, J. Lach, E. Malamud, T. Meyer, R. Poster, and W. Slater, *Phys. Rev. Lett.* 29, 1627 (1972); 30, 1151 (1973).
- ¹¹F. T. Dao, R. Hanft, J. Lach, E. Malamud, F. Nezirick, V. Davidson, A. Firestone, D. Lam,

F. Nagy, C. Peck, A. Sheng, R. Poster, P. Schlein, W. Slater, and A. Dzierba, *Phys. Rev. Lett.* 33, 389 (1974).

- ¹²R. Bouclier, G. Charpak, Z. Dimcovski, G. Fischer, F. Sauli, G. Coignet, and G. Flugge, *Nucl. Instrum. Methods* 88, 149 (1970); B. Dieterle, R. Heaphy, and M. K. Johnson, *ibid.* 116, 189 (1974); R. Bouclier *et al.*, CERN Internal Report No. NP 70-22 (unpublished); B. Makowski and B. Sadoulet, *Nucl. Instrum. Methods* 111, 561 (1973).